

Fabrication and characterization of PbIn-Au-PbIn superconducting junctions

Nam-Hee Kim, Bum-Kyu Kim, Hong-Seok Kim, and Yong-Joo Doh*

Department of Physics and Photon Science, Gwangju Institute of Science and Technology, Gwangju 61005, Korea

(Received 21 November 2016; revised or reviewed 26 December 2016; accepted 27 December 2016)

Abstract

We report on the fabrication and measurement results of the electrical transport properties of superconductor-normal metal-superconductor (SNS) weak links, made of PbIn superconductor and Au metal. The maximum supercurrent reaches up to $\sim 6 \mu\text{A}$ at $T = 2.3 \text{ K}$ and the supercurrent persists even at $T = 4.7 \text{ K}$. Magnetic field dependence of the critical current is consistent with a theoretical fit using the narrow junction model. The superconducting quantum interference device (SQUID) was also fabricated using two PbIn-Au-PbIn junctions connected in parallel. Under perpendicular magnetic field, we clearly observed periodic oscillations of dV/dI with a period of magnetic flux quantum threading into the supercurrent loop of the SQUID. Our fabrication methods would provide an easy and simple way to explore the superconducting proximity effects without ultra-low-temperature cryostats.

Keywords : Superconducting weak link, PbIn alloy, SQUID, Josephson junction

1. INTRODUCTION

Superconducting weak link, which consists of normal metal and superconducting electrodes, provides a good platform to study superconducting proximity effects [1]. Recent advancement of fabrication methods for nano-scale devices enables us to explore various quantum electronic transport phenomena in nano-hybrid mesoscopic systems combined with superconductivity [2-8]. Usually aluminum (Al) is used as a superconducting electrode because of its very long superconducting coherence length, $\xi_{\text{Al}} \sim 1.6 \mu\text{m}$. It is, however, required to maintain the sample in a ultra-low temperature ($\ll 1.2 \text{ K}$) using a dilution refrigerator, which is limited by the superconducting transition temperature, T_c , of Al ($T_c \sim 1.2 \text{ K}$). Therefore other superconducting materials with higher T_c above the liquid helium temperature are necessary for a broad and relatively easy applications of the superconducting junctions.

Herein, we report the fabrications and measurements of the SNS-type Josephson junctions, which consist of superconducting PbIn electrodes and normal-metal Au electrode. The supercurrent through the PbIn-Au-PbIn junction was observed up to $T = 4.7 \text{ K}$ and the maximum supercurrent increased monotonously with decreasing temperature. The superconducting quantum interference device (SQUID) was also fabricated using PbIn-Au-PbIn junctions and it exhibited a clear modulation of dynamic resistance, dV/dI , as a function of external magnetic field to reflect the I_c modulation behavior due to superconducting phase interference effects. Our experimental study could be utilized for the applications on various superconducting

devices such as a superconducting interferometer and a nano-hybrid SQUID working at the liquid-helium temperature.

2. EXPERIMENTALS

The PbIn-Au-PbIn weak links were fabricated in a two-step process, using conventional electron-beam lithography. Firstly, the normal-metal electrode made of Cr/Au (5/50 nm) bilayer was fabricated on the surface of Si/SiO₂ substrate. After that, 300 nm-thick PbIn electrodes are formed on top of the Au electrode using additional electron-beam lithography. The surface of Cr/Au electrode was treated in an oxygen-plasma chamber to remove any residual electron-beam resist before the deposition of PbIn film. The PbIn alloy film was deposited by evaporating a mixture of lead (Pb) and indium (In) pellets with a weight ratio of 1:1. Finally, we deposited 20 nm-thick Au capping layer on top of the PbIn film to avoid a probable formation of PbIn-oxide layer on it.

The superconducting transition temperature of the PbIn alloy film is obtained to be $T_c = 6.8 \text{ K}$ (see Fig. 1a) and the maximum critical magnetic fields are estimated to be $H_{c,\text{parallel}} = 1.2 \text{ T}$ and $H_{c,\text{perpendicular}} = 0.74 \text{ T}$ (see Fig. 1b) [9]. Figure 1c shows a scanning electron microscopy (SEM) image of PbIn-Au-PbIn Josephson junctions after the completion of the device fabrication process. The width of the Au electrode and the gap distance between two superconducting electrodes are found to be $w = 500 \text{ nm}$ and $L = 220 \text{ nm}$, respectively, for the far left junction. The measurement configuration is also depicted in Fig. 1c, where bias current is applied from I+ to I- and voltage difference is measured between V+ and V-.

* Corresponding author: yjdoh@gist.ac.kr

3. RESULTS AND DISCUSSION

Figure 1d displays the current-voltage (I - V) characteristic curve obtained from sample D1 at the base temperature, $T = 2.3$ K. It reveals a supercurrent branch without hysteresis, meaning that a superconductor-normal-superconductor (SNS) junction was well formed in the absence of a capacitive insulating interface between PbIn and Au electrodes. In our experiment, the maximum critical current, so-called a critical current (I_c), was obtained to be ~ 6.0 μA at the base temperature and the normal-state resistance was $R_N = 0.42$ Ω . The inset displays the I - V curve measured from sample D2 at $T = 2.3$ K, indicating $I_c \sim 700$ nA and $R_N = 0.83$ Ω .

Temperature-dependent I_c is displayed in Fig. 2a. I_c was determined from the I - V curve at each temperature using a linear fit crossing the zero-voltage axis. At higher temperature, I_c decreases exponentially. The I_c vs. T data near T_c are fitted well to a formula [10] of

$$I_c(T) \propto \sqrt{T} e^{-\frac{2\pi k_B T}{E_{\text{Th}}}} \quad (\text{eq.1})$$

where k_B is the Boltzmann constant and E_{Th} is the Thouless energy. We obtain $E_{\text{Th}} = 400$ μeV as a result of fitting. Since the Thouless energy is given by $E_{\text{Th}} = \hbar D/L^2$, where \hbar is the reduced Planck constant and D is a diffusion constant of Au layer, we can estimate an effective gap distance to be $L^* = (\hbar D/E_{\text{Th}})^{1/2} = 200$ nm, which is quite similar to a geometric distance $L = 220$ nm. Here we used the Fermi velocity $v_F = 1.4 \times 10^8$ cm/s [11] and the mean free path $l_{\text{mfp}} = 50$ nm to obtain $D = l_{\text{mfp}} \cdot v_F/3 = 230$ cm^2/s . We also note that l_{mfp} was obtained from a residual resistivity of Au at $T = 2.3$ K, which is $\rho_{\text{Au}} = 1.7 \times 10^{-6}$ Ωcm [12]. In addition, the superconducting coherence length is given by $\xi = (\hbar D/\Delta_{\text{PbIn}})^{1/2} = 140$ nm with the superconducting gap energy of PbIn, $\Delta_{\text{PbIn}} = 0.8$ meV [8]. Thus our PbIn-Au-PbIn junction is in a long diffusive junction limit with satisfying $l_{\text{mfp}} \ll \xi < L$ [13].

Figure 2b is the magnetic field dependence of I_c at $T = 2.3$ K. It is well known that I_c exhibits a periodic modulation with the application of the perpendicular magnetic field, *i.e.* Fraunhofer pattern, where the I_c minima occur at the integer magnetic flux quanta through the lateral area of the junction. The theoretical prediction [14] is given by $I_c(B) = I_c(0) |\sin[\pi\Phi/\Phi_0]| / (\Phi/\Phi_0)$, where Φ_0 is the magnetic flux quantum, $\Phi_0 = h/2e = 2.07 \times 10^{-15}$ Wb, and Φ is the magnetic field flux inside the junction area. However, $I_c(B)$ data (symbols) in Fig. 2b exhibit a monotonically decreasing behavior instead of a periodic modulation. The monotonous $I_c(B)$ data can be explained by the narrow junction model [15], where the junction width w is comparable to or smaller than the magnetic length $\xi_B = (\Phi_0/B)^{1/2}$ and the applied B field acts as a pair-breaker to suppress I_c .

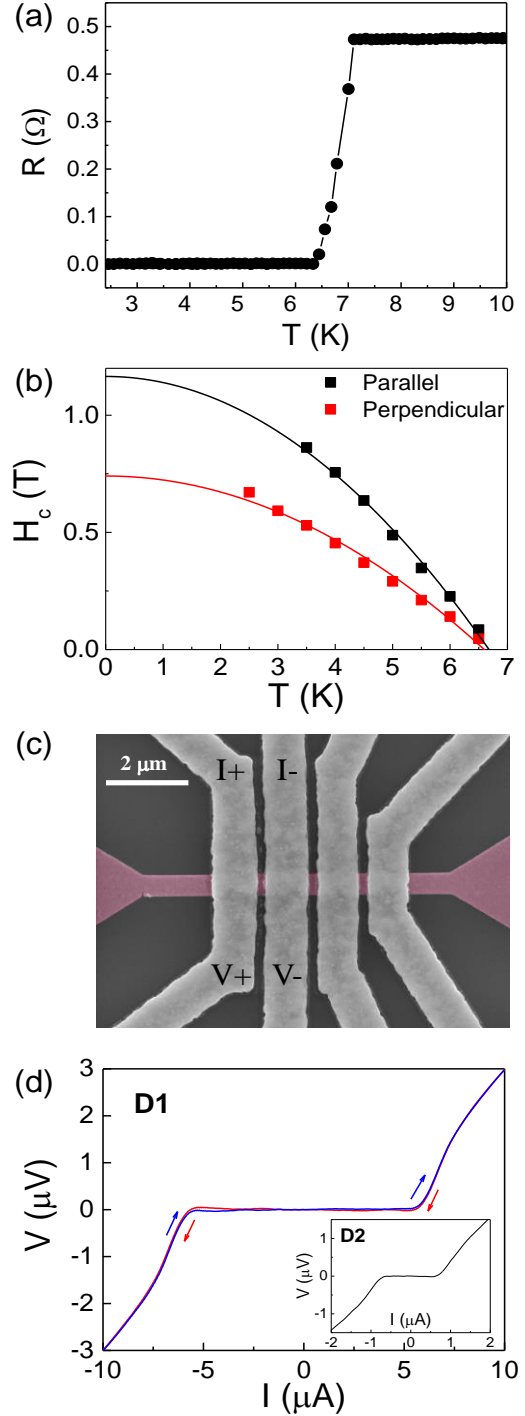


Fig. 1. (a) Temperature dependence of resistance of PbIn film. (b) Temperature-dependent critical magnetic field of PbIn film applied with parallel (black) and perpendicular (red) magnetic fields. (c) SEM image of SNS junctions with normal Au electrode (red) and superconducting PbIn electrodes (gray). (d) Current-voltage (I - V) curves of sample D1 at $T = 2.3$ K. Inset: I - V characteristic curve from sample D2 at the same temperature.

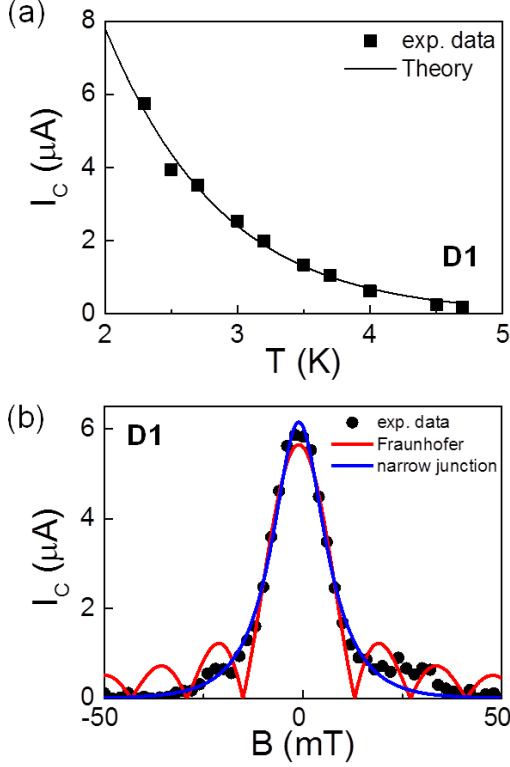


Fig. 2. (a) Temperature dependence of I_c . The solid line is a theoretical fit (see text). (b) Magnetic field dependence of I_c at $T = 2.3$ K. The red solid line represents the ideal Fraunhofer pattern, while the blue line is a fitting results using eq.(2).

TABLE DEVICE CHARACTERISTICS OF THE SNS JUNCTIONS AND SQUID.				
Sample	L (nm)	w (nm)	I_c (μ A) at $T = 2.3$ K	J_c (A/cm^2)
D1	220	540	6.0	2.2×10^4
D2	270	460	0.70	3.1×10^3
SQUID	160	570	0.34	6.0×10^2

In a narrow junction ($w < \xi_B$), the magnetic field dependence of I_c is given by [16],[13]

$$eRI_c = \frac{4\pi k_B T}{r} \sum_{n=0}^{\infty} \frac{\Delta^2 / (\Delta^2 + \omega_n^2)}{\sqrt{2 \left(\frac{\omega_n + \Gamma_B}{\varepsilon_T} \right) \sinh \left(2 \left(\frac{\omega_n + \Gamma_B}{\varepsilon_T} \right) \right)}} \quad (\text{eq.2})$$

where $r = R_B/R_N$ with the barrier resistance R_B , $R = R_N(1+2r)$, $\omega_n = (2n+1)\pi k_B T$ is the n -th Matsubara energy, and $\Gamma_B = De^2 B^2 w^2 / 6\hbar$ is the magnetic depairing energy. The blue solid line in Fig. 2b is the result of fitting with $r = 0.34$ and $L^* = 650$ nm, where L^* is an effective junction length including the magnetic penetration effect. Here we obtained the magnetic length $\xi_B = 590$ nm, resulting in $w/\xi_B = 0.92$. Similar $I_c(B)$ behavior has been observed in other narrow junction [17].

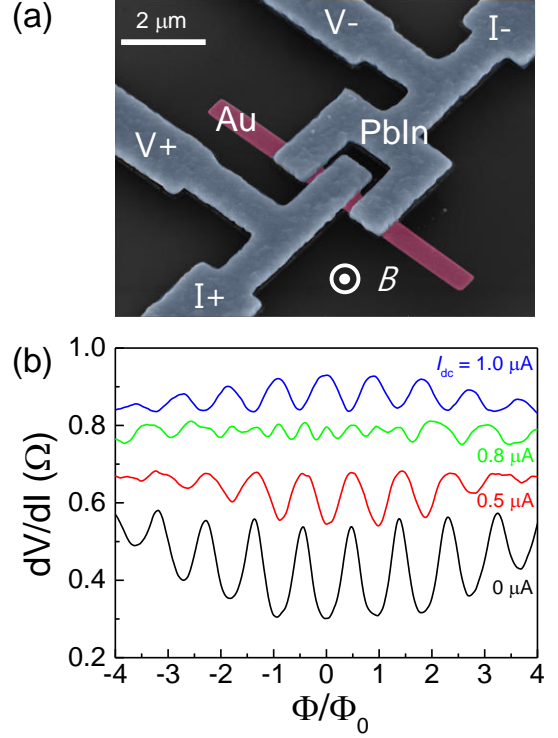


Fig. 3. (a) False-colored SEM image of SNS SQUID with Au (red) and PbIn (blue) electrodes. (b) dV/dI vs. Φ curves with varying dc current I_{dc} . The lock-in bias current was fixed at $I_{ac} = 300$ nA.

Two SNS junctions connected in parallel can form a SQUID, as depicted in Fig. 3a with the measurement configuration. Under the application of perpendicular magnetic field B , periodic modulation of dynamic resistance (dV/dI) was observed using lock-in measurement combined with dc (I_{dc}) and ac (I_{ac}) bias currents. The oscillation periodicity is obtained to be $B^* = 6.0$ Oe, resulting in $\Phi^* = 8.6 \times 10^{-16}$ Wb = $0.42 \Phi_0$ using a geometric inner-loop area of $A = 1.4 \mu\text{m}^2$. The difference of Φ^* from an expected value of Φ_0 is attributed to an effective loop area considering the London penetration depth λ_L . We can estimate λ_L from an effective loop area, $A^* = \Phi_0/B^* = 3.4 \mu\text{m}^2$, resulting in $\lambda_L = 470$ nm, which is close to the value obtained from other nanowire-based SQUID [8].

In conclusion, we have established an easy method for fabricating an SNS weak link and applied it to fabricate SQUID. We observed a dissipationless supercurrent flowing through the PbIn-Au-PbIn junction above the liquid-helium temperature. The I_c modulation with an external magnetic field resembles the one expected from the narrow junction model rather than the Fraunhofer pattern. The periodic dV/dI oscillations are clearly observed in a SQUID consisting of two PbIn-Au-PbIn junctions connected in parallel. Our experimental results would provide a useful and convenient way for exploring the superconducting phase interference effects near the liquid-helium temperatures.

ACKNOWLEDGMENT

This work was supported by the National Research Foundation of Korea through the Basic Science Research Program (Grant No. 2015R1A2A2A01006833).

REFERENCES

- [1] K. K. Likharev, "Superconducting weak links," *Reviews of Modern Physics*, vol. 51, no. 1, pp. 101-159, 1979.
- [2] Y. -J. Doh, et al., "Tunable supercurrent through semiconductor nanowires," *Science*, vol. 309(5732), pp. 272-275, 2005.
- [3] Y. -J. Doh, et al., "Andreev Reflection versus Coulomb Blockade in Hybrid Semiconductor Nanowire Devices," *Nano Letters*, vol. 8, no. 12, pp. 4098-4102, 2008.
- [4] M. Jung, et al., "Superconducting junction of a single-crystalline Au nanowire for an ideal Josephson device," *ACS Nano*, vol. 5, no. 3, pp. 2271-2276, 2011.
- [5] G. -H. Lee, et al., "Electrically tunable macroscopic quantum tunneling in a graphene-based Josephson junction," *Physical Review Letters*, vol. 107, no. 14, p. 146605, 2011.
- [6] D. Jeong, et al., "Observation of supercurrent in PbIn-graphene-PbIn Josephson junction," *Physical Review B*, vol. 83, no. 9, p. 094503, 2011.
- [7] J. -H. Choi, et al., "Complete gate control of supercurrent in graphene p-n junctions," *Nature Communications*, vol. 4, p. 2525, 2013.
- [8] H. -S. Kim, et al., "Gate-tunable superconducting quantum interference devices of PbS nanowires," *Appl. Phys. Express*, vol. 9, p. 023102, 2016.
- [9] S. -I. Park, et al., "Characterizing Pb-based superconducting thin films," *Prog. Supercond. Cryogenics*, vol. 16, no. 4, pp. 36-39, 2014.
- [10] V. Z. Kresin, "Josephson Current in Low-Dimensional Proximity Systems and the Field-Effect," *Physical Review B*, vol. 34, no. 11, pp. 7587-7595, 1986.
- [11] G. -H. Lee, et al., "Ultimately short ballistic vertical graphene Josephson junctions," *Nature Communications*, vol. 6, p. 6181, 2015.
- [12] N. W. Ashcroft and N. D. Mermin, *Solid state physics*, 1976, USA: Brooks/Cole.
- [13] F. S. Bergeret and J. C. Cuevas, "The vortex state and Josephson critical current of a diffusive SNS junction," *Journal of Low Temperature Physics*, vol. 153, no. 5-6, pp. 304-324, 2008.
- [14] M. Tinkham, *Introduction to Superconductivity*, 1996: Dover Publications.
- [15] J. C. Cuevas and F. S. Bergeret, "Magnetic interference patterns and vortices in diffusive SNS junctions," *Physical Review Letters*, vol. 99, no. 21, p. 217002, 2007.
- [16] J. C. Hammer, et al., "Density of states and supercurrent in diffusive SNS junctions: Roles of nonideal interfaces and spin-flip scattering," *Physical Review B*, vol. 76, no. 6, p. 064514, 2007.
- [17] B. -K. Kim, et al., "Very Strong Superconducting Proximity Effects in PbS Semiconductor Nanowires," ArXiv : 1607.07151, 2016.